Supplementary Information for:

Regulation of Rep helicase unwinding by an auto-inhibitory subdomain

Monika A. Makurath[1,3], Kevin D. Whitley[2,3], Binh Nguyen[4], Timothy M. Lohman[4], Yann R. Chemla[3,*]

[1]Dept. of Molecular and Integrative Physiology, University of Illinois at Urbana-Champaign, Urbana, IL, 61801, USA

[2]Center for Biophysics and Quantitative Biology, University of Illinois at Urbana-Champaign, Urbana, IL, 61801, USA

[3]Dept. of Physics, Center for the Physics of Living Cells, University of Illinois at Urbana-Champaign, Urbana, IL, 61801, USA

[4]Dept. of Biochemistry and Molecular Biophysics, Washington University School of Medicine, St. Louis, MO, 63110, USA

*To whom correspondence should be addressed.
Tel: +1 (217) 333-6501
Fax: (217) 244-7187
Email: ychemla@illinois.edu

This PDF file includes:

Supplementary Information Text
Table S1 and S2
Figs. S1 to S7
References for SI reference citations

SUPPLEMENTARY INFORMATION TEXT

Protein purification

wtRep and RepΔ2B were expressed and purified as described (1, 2). Briefly, RepΔ2B was expressed from plasmid pRepOΔ2B that encoded Rep helicase in which the 2B subdomain was removed and amino acids Thr-375 to Arg-542 were replaced with three Gly residues. wtRep and RepΔ2B had identical N-termini and were under the control of the same promoter.

DNA construct synthesis

Both hairpin and fork DNA constructs used in these experiments consisted of a variable "insert" between two long double-stranded (ds)DNA "handles" that were modified with biotin and digoxigenin to facilitate attachment to the beads. All oligonucleotides for the synthesis of the constructs were purchased from Integrated DNA Technologies (IDT, Coralville, IA), and the sequences of the primers and inserts are listed in **Table S1**. For a detailed step-by-step protocol, we refer the reader to Ref. (3).

The "hairpin" construct was made by ligating a left handle (LH, 1.5 kb) and a right handle (RH$_{hairpin}$, 1.5 kb) to an 89-bp hairpin stem capped by a (dT)$_4$ tetraloop (**Fig. S1A**). LH was prepared by PCR amplifying a section of the pBR322 plasmid (New England Biolabs, Ipswich, MA). The LH forward primer was modified with a single biotin at the 5' end in order to form a linkage to a streptavidin-coated bead. LH was digested with the restriction endonuclease PspGI (NEB) leaving a phosphorylated 5-nt 5' overhang. The phosphate group was removed by incubating the digested LH with Antarctic phosphatase (NEB). RH$_{hairpin}$ was synthesized using "auto-sticky" PCR of a different section of pBR322, using a reverse primer containing an abasic site and a 29-nt 5' overhang that annealed to the hairpin stem. The RH$_{hairpin}$ forward primer was modified with a single 5' digoxigenin to form a linkage to an anti-digoxigenin antibody-coated bead. LH, hairpin, and RH were ligated together at 24 °C for 1 hour with T4 DNA ligase (NEB). The final product contained a poly-dT ssDNA binding site for protein loading at the 3' end of the 89-bp hairpin stem. Unless otherwise noted, the loading site was 10 nt.

The "fork" construct was made by annealing and ligating four DNA fragments: a dsDNA left handle (LH, 1.5 kb) and right handle (RH$_{fork}$ 1.5 kb), a short ssDNA spacer, and a free 3' poly-dT ssDNA tail for protein loading (**Fig. S1B**). LH for the hairpin and fork constructs were identical and synthesized following the same protocol. RH$_{fork}$ was prepared by PCR amplifying a segment of lambda phage DNA (NEB). Similarly to RH$_{hairpin}$, the RH$_{fork}$ reverse primer was modified with a single digoxigenin at the 5' end. RH$_{fork}$ was digested with HgaI (NEB), leaving a 5-nt long 5' overhang. The construct was synthesized in three ligations. LH was ligated to the ssDNA spacer, which contained a complementary sequence to the LH 5' overhang, a (dT)$_4$ spacer, and a complementary sequence to the 3' ssDNA tail fragment. RH$_{fork}$ was ligated to the free 3' poly-dT ssDNA tail. Then, LH with the spacer and the RH$_{fork}$ with the free 3' end were ligated together to complete the synthesis of the construct. The final fork construct had a ssDNA protein loading site immediately adjacent to a 1,550-bp dsDNA track for protein unwinding. Unless otherwise noted, the loading site was 10 nt.

Microfluidic chamber design and construction

The sample chamber for optical tweezers measurements was made by melting a Nescofilm mask (Nescofilm; Karlan, Phoenix, AZ) between two glass microscope coverslips with precut fluid inlets and outlets. The mask and coverslip were patterned by cutting with a CO_2 laser engraver (VLS2.25, Universal Laser Systems, Sylvania, OH). The outer channels were connected with the inner channels through 25-µm ID, 100-µm OD glass capillaries (Garner Glass Co., Claremont, CA) embedded in the Nescofilm to introduce either DNA-coated streptavidin or anti-digoxigenin beads. The inner channels contain two adjacent laminar flow fluid streams to separate the protein-containing buffer from either the ATP or blank buffers. The glass coverslips were passivated with polyethylene glycol (PEG) to prevent protein adsorption. Details on chamber design and construction can be found in Ref. (3).

Optical trap measurements

All measurements were made using a custom-built dual trap optical tweezers described previously (3–5). Data were collected at a rate of 100 Hz, and all unwinding data were collected using a force feedback system to maintain a constant tension in the tethered DNA. At the start of an experiment, a DNA tether was formed in a non-protein area of the sample chamber (**Fig. S3A**) and its force-extension behavior obtained (**Fig. S1C-D**). Force-extension curves were well fit by the extensible worm-like chain (*XWLC*) model using the modified Marko-Siggia equation described in ref. (6):

$$F = \frac{k_B T}{P}\left[\frac{1}{4}\left(1 - \frac{x}{L} + \frac{F}{S}\right)^{-2} - \frac{1}{4} + \frac{x}{L} - \frac{F}{S} \right],$$

where x is the end-to-end DNA extension, F is the force, P is the persistence length, S is the stretch modulus, L is the contour length, and k_B is the Boltzmann constant and T is the temperature. Force-extension curves of molecules with dsDNA and ssDNA have extension $x_{ds}(F) + x_{ss}(F)$ where each term is given by the equation above with the following parameters: persistence length P_{ds} = 53 nm and P_{ss} = 1.2 nm, stretch modulus S_{ds} = 1,100 pN and S_{ss} = 1,000 pN, and contour length $L_{ds} = N_{ds}h_{ds}$ and $L_{ss} = N_{ss}h_{ss}$ where N_{ds} and N_{ss} are the number of dsDNA base pairs and ssDNA nucleotides, respectively, and h_{ds} = 0.34 nm bp^{-1} and h_{ss} = 0.59 nm nt^{-1} (7–9). The hairpin unzipped mechanically at an applied force of ~16 pN, and the hairpin unzipping transition was well fit by a model incorporating the base pairing energies of the exact hairpin sequence (**Fig. S1C**, black line), as described in (10, 11).

Two different experimental modes were used to measure Rep unwinding activity. Under *protein-replacement* conditions, the protein and ATP were in the same laminar flow stream in the sample chamber. A DNA tether, once formed, was moved to this stream for the duration of the measurement of Rep activity. Upon dissociation from the DNA, Rep could be replaced by other protein in solution. Under *single-turnover* conditions, the protein and ATP were in separate streams. A tether in the ATP stream was "dipped" (moved briefly) into the protein stream for 10-25 s to load a single Rep molecule, and then moved back into the ATP stream (**Fig. S3A**). Activity was detected only after exposure to ATP, and no activity was observed after protein dissociation. For some experiments, the protein stream also contained ATP-γS, as noted.

Rep activity was measured from the change in extension of the tethered DNA construct. All measurements of Rep unwinding were carried out at a constant force, with the force ranges for hairpin and fork experiments 4-14 pN and 25-55 pN, respectively. At a particular force, the change in extension

$\Delta x(t)$ in nm was converted to base pairs unwound $N_{bp}(t)$ by the following expressions: $N_{bp-hairpin}(t) = \Delta x(t) / 2\xi_{ss}(F)$ (corresponding to the release of 2 nt for each bp unwound) for the hairpin construct and $N_{bp-fork}(t) = \Delta x(t) / (\xi_{ss}(F) - \xi_{ds}(F))$ (corresponding to the conversion of 1 bp into 1 nt for each bp unwound) for the fork construct. $\xi_{ds}(F)$ and $\xi_{ss}(F)$ are the extensions of 1 bp of dsDNA and 1 nt of ssDNA at force F, respectively, given the XWLC model and the parameters listed above.

We used a general and systematic set of criteria to distinguish protein activity from noise. We first determined the background noise in our data traces by calculating the standard deviation of the extension of the DNA tether before protein activity. Events were scored as protein activity if their amplitude was >1.5× the standard deviation of the background, and if they comprised of more than 4 consecutive data points (>0.04 s).

Analysis

Unwinding speed. All wtRep and RepΔ2B fork data traces at 100 Hz were first smoothed with a 1st-order Savitzky-Goley filter. For each individual round of activity, we determined the instantaneous speed by fitting the data to a 1st-degree polynomial over 2-ms (for all hairpin data) or 4-ms (for all fork data) half-overlapping windows. The slope for each fit over each window was recorded as the instantaneous speed over that time window.

Speeds during pauses, strand-switching, and rezipping periods were excluded from the analysis as follows. To remove pauses, we first determined the standard deviation of the speed, s_{base}, during baseline periods with no helicase activity. These were selected from time periods during which the DNA extension changed less than a predefined, empirical threshold ranging from 1.5 to 8 bp, depending on the force and DNA geometry. We removed all instantaneous speeds that fell between ±1.5 × s_{base}. Additionally, we excluded speeds during strand-switching events by comparing instantaneous speeds in consecutive time windows. Strand-switching events were identified from speeds that switched from positive to negative (from unwinding to rezipping) and *vice versa* (from rezipping to unwinding). We removed instantaneous speeds in up to ±3 time windows adjacent to each identified strand-switching event.

To obtain the average unwinding speed of an individual molecule, we averaged all the positive instantaneous velocity measurements that did not correlate with regions of pauses or strand-switching. We then averaged the speed over all molecules at a particular force.

Strand-switching distance. To identify strand-switching locations we compared the local instantaneous velocity around an event of reversal in direction of protein motion on the DNA. For all our reported measurements, we considered only reversals in direction, i.e. strand-switching events from unwinding-to-rezipping, for which the positive speed was followed by negative speed. We measured strand-switching distances starting from the baseline or from the last rezipping-to-unwinding strand-switching event. For all the activity on the hairpin DNA substrate, we excluded events where reversals in direction occurred due to unwinding of the entire 89-bp stem of the hairpin. In these events, the DNA rezipped behind the protein after it translocated passed the 4-dT hairpin cap, as opposed to DNA rezipping after strand-switching.

Probabilities of helicase behavior. To compare the frequency of events that limit processivity, we considered patterns of behaviour in the data corresponding to unwinding, rezipping, strand-switching, dissociation, or snap-back. We analyzed traces from all datasets across 0.5-0.8 k_BT destabilization energy. The branching probabilities were calculated separately for wtRep, RepΔ2B hairpin and RepΔ2B fork activity. A branching probability was calculated for each possible behavior at two branch points (**Fig. 5**): 1) termination of unwinding and 2) restart of unwinding after rezipping.

At the first branch point (**Fig. 5**, rightmost schematic), we counted the number of times the helicase either strand-switched, which was followed by duplex rezipping behind the helicase, or dissociated, which was followed by characteristic rapid and spontaneous duplex rezipping to the baseline. At the second branch point (**Fig. 5**, leftmost schematic), we counted the number of times the helicase either dissociated after reaching the baseline, strand-switched from rezipping-to-unwinding in the middle of the DNA substrate, or snapped-back to the start site. The two latter behaviors were followed by restart of unwinding. We did not quantify branching probabilities for events past the first round of unwinding because of the limited statistics, i.e. the second or later rounds of activity happened only for a fraction of the traces.

Modelling

Destabilization energy. RepΔ2B unwinding data were collected on hairpin and fork DNA over differing force ranges, 4-14 pN and 25-55 pN, respectively (**Fig. 1-4**). To compare the results obtained on the hairpin and fork constructs, we determined the effect of force on duplex stability in the two construct geometries. The force-induced destabilization energy per base pair at each force was calculated from the expressions:

$$\Delta G_{hairpin}(F) = 2\int_0^F dF' \, \xi_{ss}(F') \tag{1}$$

corresponding to the energy of stretching 2 nt released by unwinding 1 bp, for the hairpin construct, and

$$\Delta G_{fork}(F) = \int_0^F dF' \left(\xi_{ss}(F') - \xi_{ds}(F') \right) \tag{2}$$

corresponding to the energy difference stretching 1 nt and 1 bp, for the fork construct.

Force-dependence of Rep unwinding speed. RepΔ2B and wtRep unwinding speeds show a dependence on force (**Fig. 3**), with RepΔ2B speeds on two construct geometries—hairpin and fork DNA—overlapping when plotted against force-induced destabilization energy $\Delta G(F)$. Data sets of RepΔ2B on hairpin and fork DNA and of wtRep on hairpin DNA were well fit to a single model adapted from the theoretical approach developed by Betterton and Jülicher (12). Briefly, the unwinding speed v_u is given by the translocation speed v_{trans}, i.e. the helicase speed in the absence of a duplex to unwind, multiplied by a factor less than one that quantifies the effects of duplex stability and helicase-DNA interactions

$$v_u(F) = v_{trans} \left(\frac{c + (1-c)e^{-fU_{int}/k_BT}}{c + (1-c)e^{-U_{int}/k_BT}} \, c \right) \tag{3}$$

5

Here, U_{int} is the interaction energy between helicase and DNA fork that destabilizes the duplex, and f is a parameter with range $0 < f < 1$ that determines whether the interaction accelerates duplex opening ($f = 0$) or decreases duplex closing ($f = 1$). c is the probability for the duplex to open a given number of base pairs for the helicase to step forward, given by a Boltzmann factor with free energy

$$\Delta G = n\left(\Delta G_{bp} - \Delta G(F)\right) \tag{4}$$

where n is the number of unwound base pairs required, ΔG_{bp} is the free energy of forming each base pair, and $\Delta G(F)$ represents the force-induced destabilization of each base pair, given by Eq. (1) and (2) for the two DNA constructs. The average ΔG_{bp} is ~2.5 $k_B T$. We expect $n \leq d$ where d is the unwinding step size.

RepΔ2B and wtRep unwinding speeds are fit to the model combining Eq. (3) and (4) (**Fig. 3**, solid magenta and dark blue line, respectively). A value of $n \sim 2$ bp was used for both fits; prior bulk kinetic and single-molecule assays estimate the unwinding step size to be in the range d = 4-5 bp (13, 14), which satisfies $n < d$. **Table S2** summarizes the fitting parameters used to model RepΔ2B and wtRep. We note that v_{trans} matches closely with previously reported ssDNA translocation speeds for both proteins (2). Also, our parameters suggest that U_{int} is ~0.5 $k_B T$ higher for wtRep compared to RepΔ2B, which may be due to the known 2B interactions with the duplex.

Kinetic competition model of strand-switching. Our results show that as Rep helicase unwinds, it can exhibit off-pathway behaviors such as dissociation, snap-back, and, the majority of the cases, strand-switching (**Fig. 5**). To model the kinetics of strand-switching events, we assume that the helicase transitions to conformational states necessary to initiate strand-switching (e.g. formation of non-canonical protein-DNA contacts) at a rate k_{ss}. At any point, the probability p of strand-switching is given by the kinetic competition between this rate k_{ss} and the rate at which the helicase instead continues to step forward $k_u = v_u/d$, $p = k_{ss}/(k_{ss} + k_u)$. The number of steps taken until a strand-switching event occurs can be shown to be

$$N_{ss} = \frac{1-p}{p} = \frac{k_u}{k_{ss}}$$

and the corresponding distance is

$$x_{ss} = d\frac{1-p}{p} = v_u T_{ss} \tag{5}$$

where $T_{ss} = 1/k_{ss}$ is the mean time and $v_u(F)$ is the force-dependent unwinding velocity in Eq. (3).

The wtRep strand-switching distance is well fit by the simple model in Eq. (5) assuming a value of k_{ss} independent of force (**Fig. 4**, dark blue line; see **Table S2**). The force-dependence of the strand-switching distance for wtRep is thus entirely due to that of the unwinding speed. In contrast, we found it necessary to have $k_{ss}(F)$ decrease with force to match this model to the RepΔ2B strand-switching data. This decrease could result from high duplex stability promoting strand-switching. In this mechanism, force would destabilize the duplex, reducing k_{ss}. We would expect the following dependence on force

$$k_{ss}(F) = k_{ss}(0)\exp\left(-\frac{n\Delta G(F)}{k_B T}\right)$$

with $\Delta G(F)$ given by Eq. (1) and (2) for the two experimental constructs. Such a model describes the data well (**Fig. 4**, magenta line) for both constructs, using a value of $n = 2$ bp as above. Another mechanism of force dependence in which force disrupts protein-DNA contacts necessary for strand-switching is less plausible. To ensure that the mean strand-switching distance for hairpin and fork DNA are the same, such a mechanism would have to produce the same values for the rate constant $k_{ss}(F)$ despite the different force ranges 4-14 pN vs. 25-55 pN.

Hairpin	
Name	**Sequence**
LH forward primer	5' - /5Biosg/TGAAGTGGTGGCCTAACTACGCAA - 3'
LH reverse primer	5' - CAAGCCTATGCCTACAGCAT - 3'
RH forward primer	5' - /5DigN/CAACAACGTTGCGCAAACT - 3'
RH reverse primer	5' - /5Phos/TTGAAATACCGACCGCTCAGCTATCAGCC **TTTTTTTTTT** /idSp/CTCTGACACATGCAGCTCCC - 3'
Hairpin insert	5' -/5Phos/CCTGGGGCTGATAGCTGAGCGGTCGGTATTTCAAAAG TCAACGTACTGATCACGCTGGATCCTAGAGTCAACGTACTGATCA CGCTGGATCCTATTTTTAGGATCCAGCGTGATCAGTACGTTGACT CTAGGATCCAGCGTGATCAGTACGTTGACTT - 3'
Fork	
Name	**Sequence**
LH forward primer	5' - /5Biosg/TGAAGTGGTGGCCTAACTAC - 3'
LH reverse primer	5' - CAAGCCTATGCCTACAGCAT - 3'
RH forward primer	5' - /5DigN/GGGCAAACCAAGACAGCTAA - 3'
RH reverse primer	5' - CGTTTTCCCGAAAAGCCAGAA - 3'
3' overhang	5' - /5Phos/GTGAGGCCAGTGGG **TTTTTTTTTT** - 3'
4 dT spacer	5' - /5Phos/CCTGGTTTTCCCACTGGC - 3'

Table S1. Oligonucleotides for synthesizing hairpin and fork constructs. All sequences are listed in the format used by IDT. The poly-dT protein loading sites are indicated in bold and have a length of 10 nt. Constructs with extended poly-dT protein loading sites are noted in the text.

	RepΔ2B	wtRep
n	2.1 ± 0.3 bp	~2 bp
f	~0	~0
U_{int}	3.25 ± 0.6 k_BT	3.75 ± 0.5 k_BT
v_{trans}	612 ± 24 bp s^{-1}	218 ± 21 bp s^{-1}
$k_{ss}(0)$	~13 s^{-1}	16 ± 3 s^{-1}

Table S2. Model fit parameters. Error bars represent 95% confidence intervals.
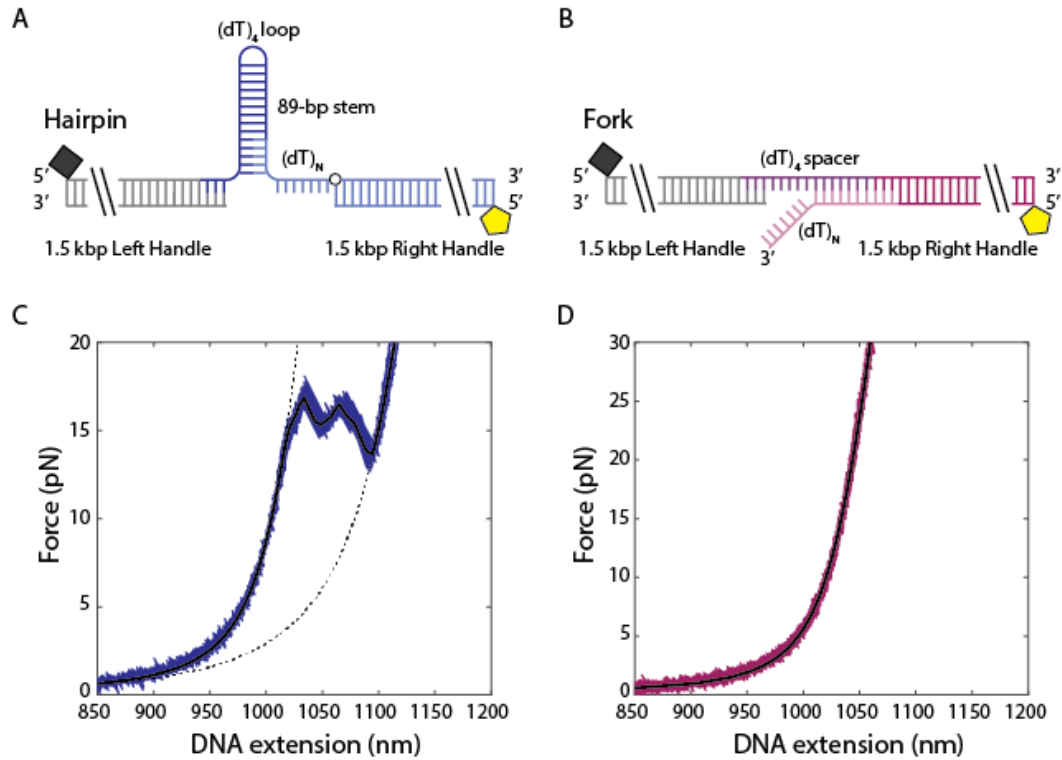
Figure S1. Hairpin and fork DNA construct design and force-extension behavior. (**A**) The hairpin construct consists of two double-stranded DNA handles (grey and light blue) ligated to a DNA hairpin which has an 89-bp stem and $(dT)_4$ loop (dark blue). At the 3' end of the hairpin, a $(dT)_N$ ssDNA section ($N = 10$ or 38 nt as noted) serves as a protein loading site and is separated from the right handle by a single abasic site (white circle). A 5' biotin (black square) and 5' digoxigenin (yellow pentagon) are used to attach DNA to streptavidin- and anti-digoxigenin-coated beads, respectively. (**B**) The fork construct consists of two double-stranded DNA handles (grey and dark magenta) ligated to two short segments making up the DNA fork structure. The top (purple) single-stranded segment is short (4 poly-dT) and has complementary overhangs to the left handle and the bottom (light magenta) single-stranded segment. The bottom (light magenta) segment contains a 3' $(dT)_N$ ssDNA tail ($N = 10$ or 20 nt as noted) for protein loading and has complementary sticky-ends to the spacer and the right handle. (**C**) Overlaid representative force-extension curves of hairpin DNA (dark blue). The force-extension curves are fitted to the XWLC model for fully closed and open hairpin (black dotted lines) and to a model of hairpin unfolding using nearest-neighbor base-pairing energies (black solid line). (**D**) Overlaid representative force-extension curves of fork DNA (dark magenta) fitted to the XWLC model (solid black line). See SI Text for details.
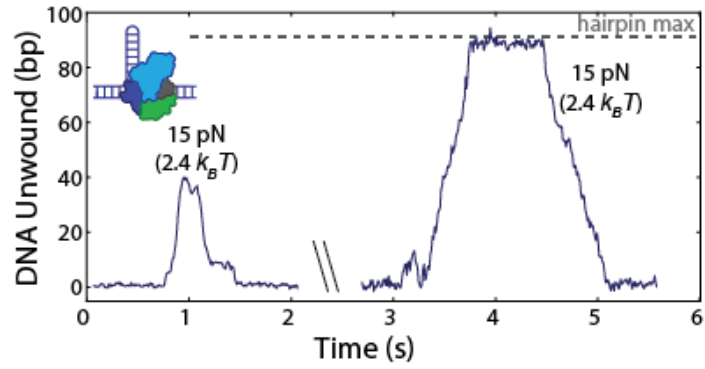
Figure S2. Representative data traces of wtRep monomer activity on the hairpin DNA substrate. wtRep monomer activity on hairpin DNA with 10-dT loading site and at protein concentration of 8.8 nM. The grey dashed line represents the limit posed by the length of the hairpin. Forces applied and corresponding destabilization energies (see SI Text) are indicated above each trace.
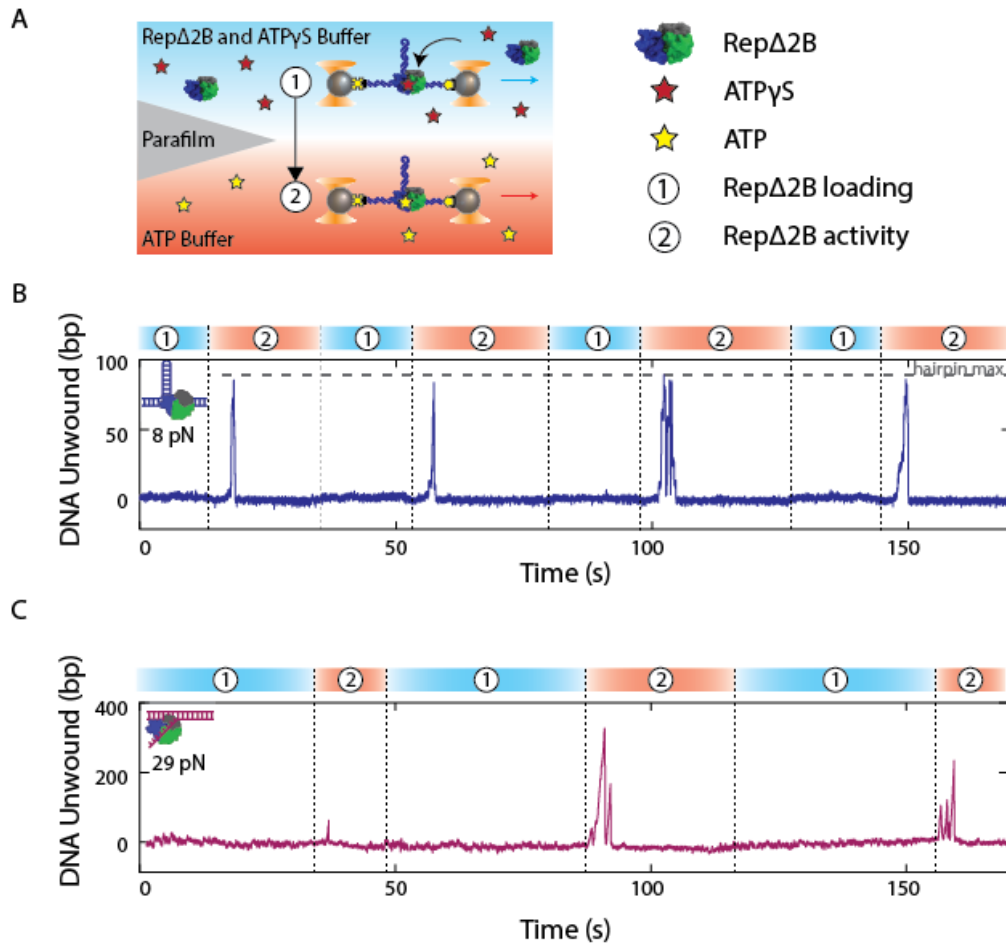
Figure S3. Schematic and representative data traces of single-turnover RepΔ2B experiments. (A) Schematic of the laminar flow chamber during single-turnover experiments. The top channel (blue) contains RepΔ2B and ATP-γS for all hairpin experiments, or only RepΔ2B for all fork experiments. After protein loading (step 1), the trapped beads and tethered DNA is moved to the bottom channel (red) containing ATP where protein activity is recorded (step 2). **(B - C)** Representative data traces illustrating consecutive loading and unwinding of RepΔ2B monomers on either the hairpin (**B**, blue) or fork (**C**, magenta) constructs. The force at which each DNA tether was held is displayed in the upper left corner.
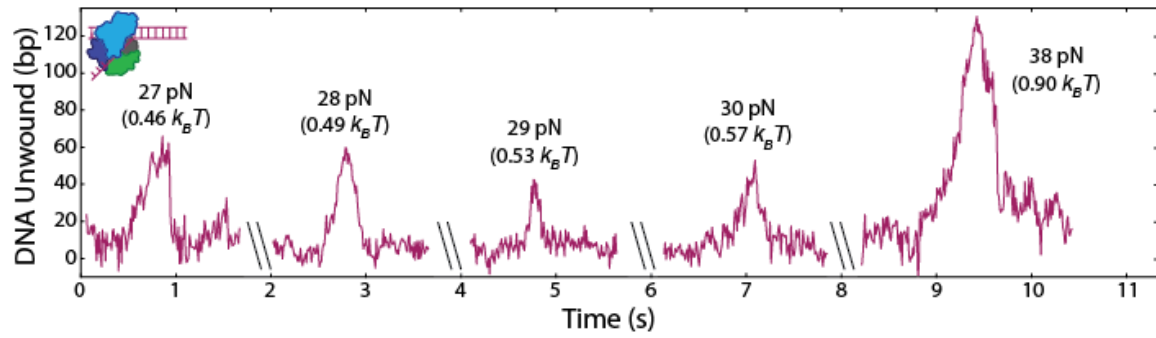
Figure S4. Representative data traces of wtRep dimer activity on the fork DNA substrate. wtRep dimer activity on fork DNA with a 20-dT loading site and at protein concentration of 35 nM. Forces applied and corresponding destabilization energies (see SI Text) are indicated above each trace.
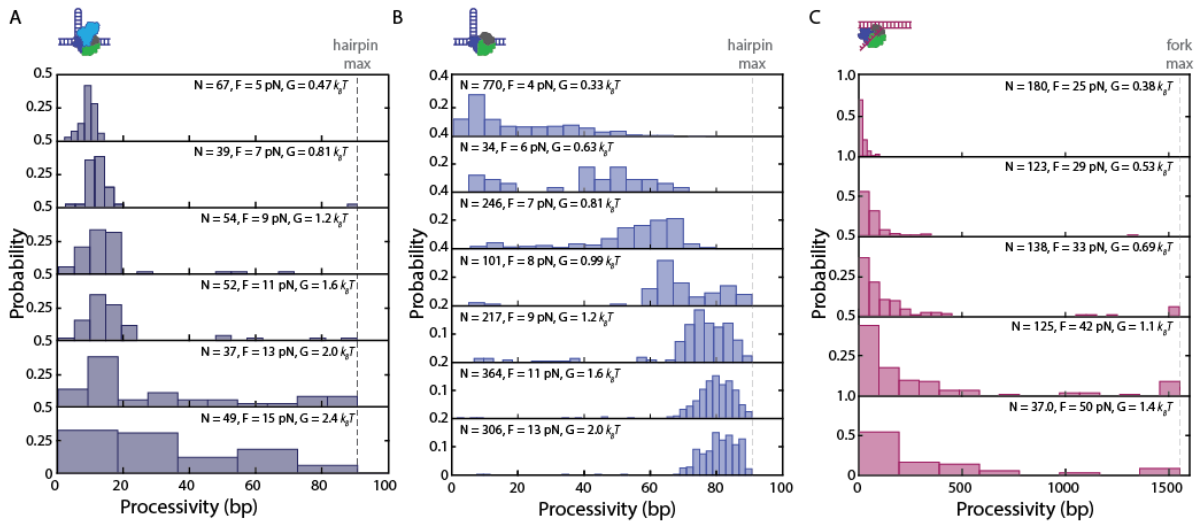
Figure S5. Distributions of unwinding processivity for wtRep dimer and RepΔ2B monomer. (**A–C**) Processivity distributions for wtRep hairpin unwinding (**A**), RepΔ2B hairpin unwinding (**B**), and RepΔ2B fork unwinding (**C**). The number of individual measurements (*N*), the force (*F*) and destabilization energy (Δ*G*) are displayed for each distribution. The dotted grey lines indicate the limits imposed by the length of the hairpin (**A, B**) and fork (**C**) substrates.
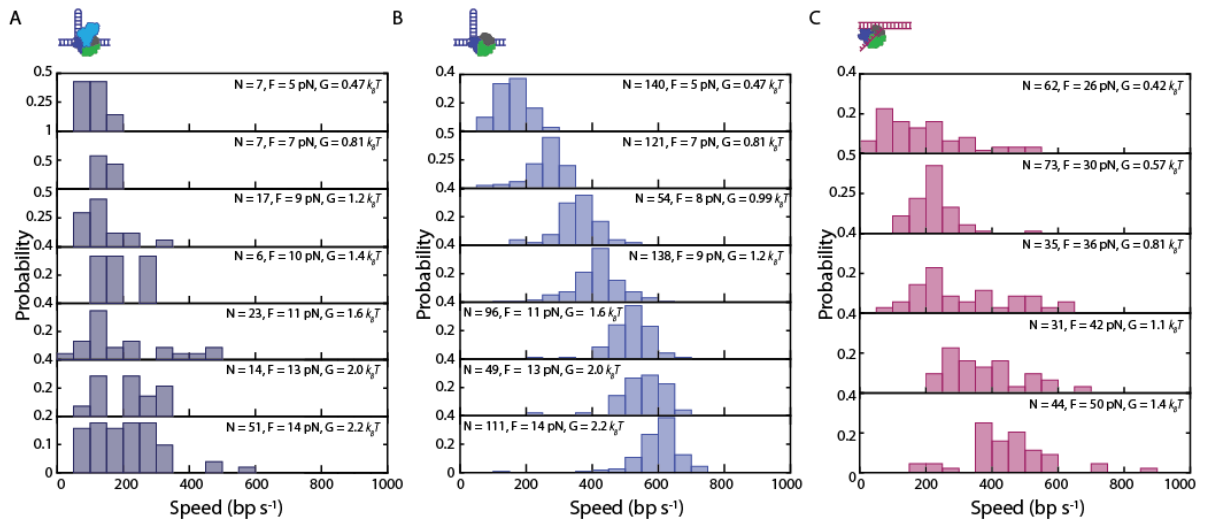
Figure S6. Distributions of unwinding speed for wtRep dimer and RepΔ2B monomer. (**A-C**) Speed distributions for wtRep hairpin unwinding (**A**), RepΔ2B hairpin unwinding (**B**), and RepΔ2B fork unwinding (**C**). The number of individual measurements (*N*), the force (*F*) and destabilization energy (Δ*G*) are displayed for each distribution.
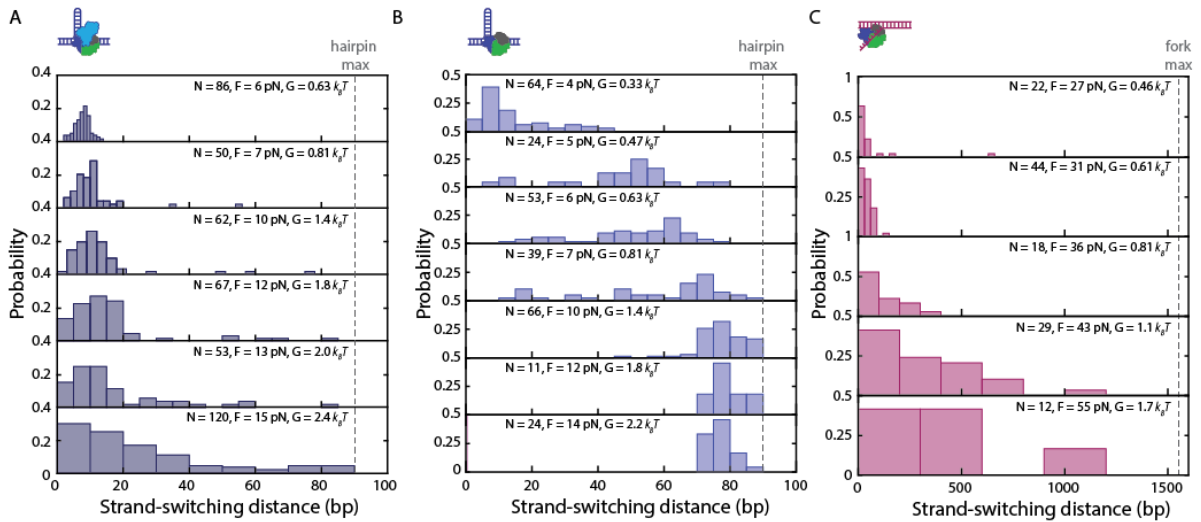
Figure S7. Distributions of strand-switching distance for wtRep dimer and RepΔ2B monomer. (**A-C**) Strand-switching distance distributions for wtRep hairpin unwinding (**A**), RepΔ2B hairpin unwinding (**B**), and RepΔ2B fork unwinding (**C**). The number of individual measurements (*N*), the force (*F*) and destabilization energy (Δ*G*) are displayed for each distribution. The dotted grey lines indicate the limits imposed by the length of the hairpin (**A, B**) and fork (**C**) substrates.

References

1. Cheng,W., Hsieh,J., Brendza,K.M. and Lohman,T.M. (2001) E. coli Rep oligomers are required to initiate DNA unwinding in vitro. *J. Mol. Biol.*, **310**, 327–350.

2. Brendza,K.M., Cheng,W., Fischer,C.J., Chesnik,M.A., Niedziela-Majka,A. and Lohman,T.M. (2005) Autoinhibition of Escherichia coli Rep monomer helicase activity by its 2B subdomain. *Proc. Natl. Acad. Sci.*, **102**, 10076–10081.

3. Whitley,K.D., Comstock,M.J. and Chemla,Y.R. (2017) High-resolution optical tweezers combined with single-molecule confocal microscopy. In *Methods in Enzymology*. Elsevier Inc., Vol. 582, pp. 137–169.

4. Moffitt,J.R., Chemla,Y.R., Izhaky,D. and Bustamante,C. (2006) Differential detection of dual traps improves the spatial resolution of optical tweezers. *Proc. Natl. Acad. Sci. U. S. A.*, **103**, 9006–9011.

5. Comstock,M.J., Ha,T. and Chemla,Y.R. (2011) Ultrahigh-resolution optical trap with single-fluorophore sensitivity. *Nat. Methods*, **8**, 335–340.

6. Wang,M.D., Yin,H., Landick,R., Gelles,J. and Block,S.M. (1997) Stretching DNA with optical tweezers. *Biophys. J.*, **72**, 1335–46.

7. Odijk,T. (1995) Notes: Stiff Chains and Filaments under Tension. *Macromolecules*, **28**, 7016–7018.

8. Marko,J.F. and Siggia,E.D. (1995) Stretching DNA. *Macromolecules*, **28**, 8759–8770.

9. Camunas-Soler,J., Ribezzi-Crivellari,M. and Ritort,F. (2016) Elastic Properties of Nucleic Acids by Single-Molecule Force Spectroscopy. *Annu. Rev. Biophys.*, **45**, 65–84.

10. Qi,Z., Pugh,R.A., Spies,M. and Chemla,Y.R. (2013) Sequence-dependent base pair stepping dynamics in XPD helicase unwinding. *Elife*, **2013**, 1–23.

11. Woodside,M.T., Behnke-Parks,W.M., Larizadeh,K., Travers,K., Herschlag,D. and Block,S.M. (2006) Nanomechanical measurements of the sequence-dependent folding landscapes of single nucleic acid hairpins. *Proc. Natl. Acad. Sci.*, **103**, 6190–6195.

12. Betterton,M.D. and Jülicher,F. (2005) Opening of nucleic-acid double strands by helicases: Active versus passive opening. *Phys. Rev. E - Stat. Nonlinear, Soft Matter Phys.*, **71**, 1–11.

13. Ali,J.A. and Lohman,T.M. (1997) Kinetic measurement of the step size of DNA unwinding by Escherichia coli UvrD helicase [published erratum appears in Science 1997 Apr 4;276(5309):21]. *Science (80-.).*, **275**, 377–380.

14. Dessinges,M.-N., Lionnet,T., Xi,X.G., Bensimon,D. and Croquette,V. (2004) Single-molecule assay reveals strand switching and enhanced processivity of UvrD. *Proc. Natl. Acad. Sci. U. S. A.*, **101**, 6439–44.